MIT Open Access Articles

Implementation of 2-bit multiplier based on electro-optic effect in Mach–Zehnder interferometers

Massachusetts Institute of Technology

CrossMark

Implementation of 2-bit multiplier based on electro-optic effect in Mach–Zehnder interferometers

Santosh Kumar[1] · Ashish Bisht[1] · Gurdeep Singh[1] ·
Angela Amphawan[2,3]

Abstract   This paper demonstrates the structure and working principle of an optical 2-bit multiplier using lithium niobate ($LiNbO_3$) based Mach–Zehnder interferometer (MZI). The powerful ability of MZI structures to switch the optical signal from one output port to the other output port has been used in the implementation of the proposed 2-bit multiplier. The paper constitutes the mathematical description of the 2-bit multiplier and thereafter compilation using MATLAB. The study is carried out by simulating the proposed device with Beam propagation method (BPM).

Keywords   Lithium niobate · Mach–Zehnder interferometer · Beam propagation method

1 Introduction

As the demand for data traffic in ultra-fast communication networks has increased, it is required to perform the signal processing and switching in optical domain. Due to the unmatched speed of photon and its ability to store a data packet in a signal of zero mass, the computing techniques using optics may lead to a way out of the limitation of computational complexity inherent in electronics. Optical multiplication has the promising applications in optical computing and communication systems. Numerous arithmetic and

✉ Santosh Kumar
  santoshrus@yahoo.com

  Angela Amphawan
  angelaoptics@gmail.com

[1] Department of Electronics and Communication Engineering, Photonics Lab, DIT University, Dehradun 248009, Uttarakhand, India

[2] Fulbright Research Fellow, Massachusetts Institute of Technology, Cambridge, MA 02139, USA

[3] InterNetWorks Research Laboratory, School of Computing, Universiti Utara Malaysia, 06010 Sintok, Kedah, Malaysia

logic operations have been suggested in the field of optical computing (Li et al. 1999; Sokoloff et al. 1993; Wang et al. 2002; Shen and Wu 2008; Vikram and Caulfield 2005). Design of all-optical multiplication technique with non-linear medium has been demonstrated (Mukhopadhyay et al. 2001). An all-optical 2-bit multiplication using Semiconductor optical amplifier (SOA)-assisted Sagnac Switch has been implemented using an optical half adder and optical AND gate (Gayen et al. 2010). An exclusive scheme to implement an all-optical AND logic gate and half adder circuit which are the primary building blocks of the multiplier circuit using non-linear shifting operation and frequency conversion properties of semiconductor optical amplifier (SOA) (Mandal et al. 2014). The optical logic operation in a sagnac interferometer with electro-optic modulation has been studied (Li et al. 2014). Design of 1×4 signal router by using $LiNbO_3$ based Mach–Zehnder Interferometers (MZIs) has been proposed in which authors have also explained the basic switching phenomenon due to electro-optic effect inside MZI (Raghuwanshi et al. 2013). The voltage applied to the electrodes deposited on the integrated MZI, creates an electric field distribution within the substrate, which consequently changes its refractive index. Due to variation of the refractive index, the phase difference arises, and depending upon the phase, signal shifts from one waveguide to another waveguide. $LiNbO_3$ based MZI is characterized by the attractive features of compact size, thermal stability (Wooten et al. 2000), re-configurability (Jin et al. 2014), integration potential (Wooten et al. 2000), low latency and low power consumption (Singh et al. 2012; Kumar Kumar et al. 2015b). Due to which many researchers have shown their keen interest and implemented various combinational and sequential circuits using MZIs (Kumar et al. 2013, 2014a, b, 2015a, b; Raghuwanshi et al. 2013, 2014). The analysis of various factors such as crosstalk, extinction ratio (ER), power imbalance and transition loss has been demonstrated (Kumar et al. 2014b).

This paper outlines the design process of 2-bit multiplier based on the electro-optic effect of integrated MZI. The multiplier is implemented with the help of MZIs in MATLAB and its results are verified with the Beam propagation method (BPM). The basic working principle, mathematical formulation and MATLAB simulation of the proposed 2-bit multiplier is presented in Sect. 2. The result obtained through BPM and their discussions are well presented in Sect. 3. Section 4 presents the analysis of some factors influencing the performances of proposed device. Finally, Sect. 5 comprises the conclusion.

2 Implementation of the 2-bit multiplier using the MZIs

The application of 2-bit multiplier is essential in order to improve the flexibility in the complex digital circuits. There are fourteen MZIs required to implement the 2-bit multiplier shown in Fig. 1. The optical signal is provided to the first input port of MZI1. The output port of first MZI is directly connected to the first input port of MZI3. The first output port of MZI3 is assigned as M_0. The control signal A_0 is given to MZI1 and B_0 is given to MZI3. So, LSB of multiplier, $M_0 = A_0 \cdot B_0$. Another optical signal is given to MZI4, which is connected to MZI7. The output of MZI7 is connected to PIN Photo-detector, it converts the optical signal to electrical signal, then an amplifier amplifies this signal and given to MZI10 and MZI11 as a control signal (control signal $B_0 \cdot A_1$). The control signal B_0 and A_1 is given to MZI4 and MZI7 respectively. Similarly, the other optical signal is given to the first input port of MZI2 (control signal A_0), which is connected to the first input port of
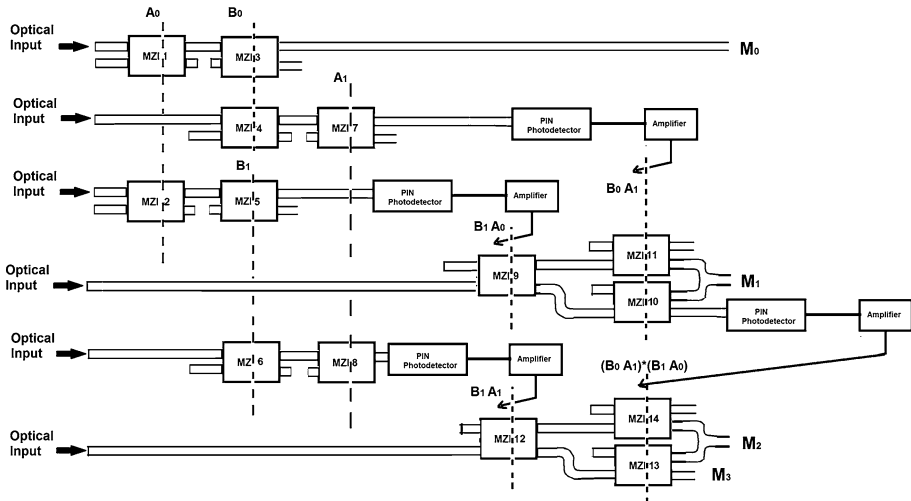
Fig. 1 Schematic diagram of two-bit multiplier using the MZIs

MZI5 (control signal B_1), and output of MZI5 is given to PIN Photo-detector and amplifier, which is a control signal of MZI9 (control signal $B_1 \cdot A_0$). An optical signal is given to second input port of MZI9, which first output is connected to the second input port of MZI11 and the second output port of MZI9 is given to the second electrode of MZI10. The second output port of MZI11 and the first output port of MZI10 is collectively assigned as M_1. Here, the second output of MZI10 is connected to PIN Photo-detector and amplifier, whose output is given as a control signal $(B_0 \cdot A_1) \cdot (B_1 \cdot A_0)$ to MZI13 and MZI14. One more control signal $(B_1 \cdot A_1)$ is obtained in a similar fashion from MZI6 and MZI8, which is given to the second electrode of MZI12. The other optical signal launches to MZI12, which is connected to MZI13 and MZI14. The second output port of MZI14 and the first output port of MZI13 is collectively given the result of M_2. Finally, the second output port of MZI13 is given as M_3. Here, M_0 is LSB (Least significant Bit) and M_3 is consider as the MSB (Most significant Bit).

2.1 Mathematical formulation of normalized power at various output ports

For all possible minterms at the output port M_0, M_1, M_2 and M_3 (to perform the 2-bit multiplication), the normalized power can be written as (calculated in "Appendix").
At Port M_0;

$$M_0 = \left| \frac{OUT1_{MZI3}}{E_{in}} \right|^2 = \left\{ \sin^2 \left(\frac{\Delta\varphi_{MZI1}}{2} \right) \sin^2 \left(\frac{\Delta\varphi_{MZI3}}{2} \right) \right\} \tag{1}$$

At Port M_1;

$$M_1 = \left\{ \sin^2 \left(\frac{\Delta\varphi_{MZI9}}{2} \right) \cos^2 \left(\frac{\Delta\varphi_{MZI10}}{2} \right) \right\} + \left\{ \cos^2 \left(\frac{\Delta\varphi_{MZI9}}{2} \right) \sin^2 \left(\frac{\Delta\varphi_{MZI11}}{2} \right) \right\} \tag{2}$$

At Port M$_2$;

$$M_2 = \left\{ \sin^2\left(\frac{\Delta\varphi_{MZI12}}{2}\right) \cos^2\left(\frac{\Delta\varphi_{MZI13}}{2}\right) \right\} + \left\{ \cos^2\left(\frac{\Delta\varphi_{MZI12}}{2}\right) \sin^2\left(\frac{\Delta\varphi_{MZI14}}{2}\right) \right\} \quad (3)$$

At Port M$_3$;

$$M_3 = \left|\frac{OUT2_{MZI13}}{E_{in}}\right|^2 = \left\{ \sin^2\left(\frac{\Delta\varphi_{MZI12}}{2}\right) \sin^2\left(\frac{\Delta\varphi_{MZI13}}{2}\right) \right\} \quad (4)$$

Figures 2a–d show MATLAB simulation results of 2-bit multiplier, where column 1 represents B_1. Similarly, columns 2, 3 and 4 represent bits B_0, A_1 and A_0 respectively. Outputs M_3, M_2, M_1 and M_0 are shown in columns 5, 6, 7 and 8 respectively.

3 Implementation of the 2-bit multiplier using the BPM

Further extending, OptiBPM is used to analyze the proposed structure. OptiBPM basically works on the principle of FD-BPM (Raghuwanshi et al. 2013). BPM allows computer-simulated observation of the light-field distribution. The radiation and the guided field can be examined simultaneously. All these phenomena along with digital computation techniques, e.g. multiplier can be easily implemented by the proper combination of Mach–Zehnder interferometers.

3.1 2-Bit multiplication operation

The result of 2-bit multiplier obtained from the BPM is shown in Fig. 3a–d. It can be verified by Table 1, which is the truth table of 2-bit multiplier obtained from the MATLAB (shown in Fig. 2a–d). The different combinations of control signals are applied to the proposed device as shown in Fig. 1 and their corresponding responses can be discussed as follows.

MZI9 is controlled by the control signal $X_1 = (B_1 \cdot A_0)$.
MZI10 and MZI11 are controlled by the control signal $X_2 = (B_0 \cdot A_1)$.
MZI12 is controlled by the control signal $X_3 = (B_1 \cdot A_1)$.
MZI13 and MZI14 are controlled by control signal $X_4 = (X_1 \cdot X_2)$.

For each combination of control signals, input optical signal of same wavelength is fed to six MZIs (MZI1, MZI2, MZI4, MZI6, MZI9, and MZI12) at the same time.

3.1.1 Case 1: $B_1 = 0$, $B_0 = 0$, $A_1 = 0$, $A_0 = 0$

Optical signals feeding to above mentioned six MZIs are terminated at the second port of MZI1, MZI2, MZI4, MZI6 because the control signal to these MZIs are LOW (Raghuwanshi et al. 2013). Incoming optical signal to MZI9 and MZI12 are terminated at first output port of MZI11and MZI14 respectively as shown in Fig. 1. Hence there is no optical signal at any output port as shown in Fig. 3a, which verifies the product of 2 bit numbers.

(a)

(b)

(c)
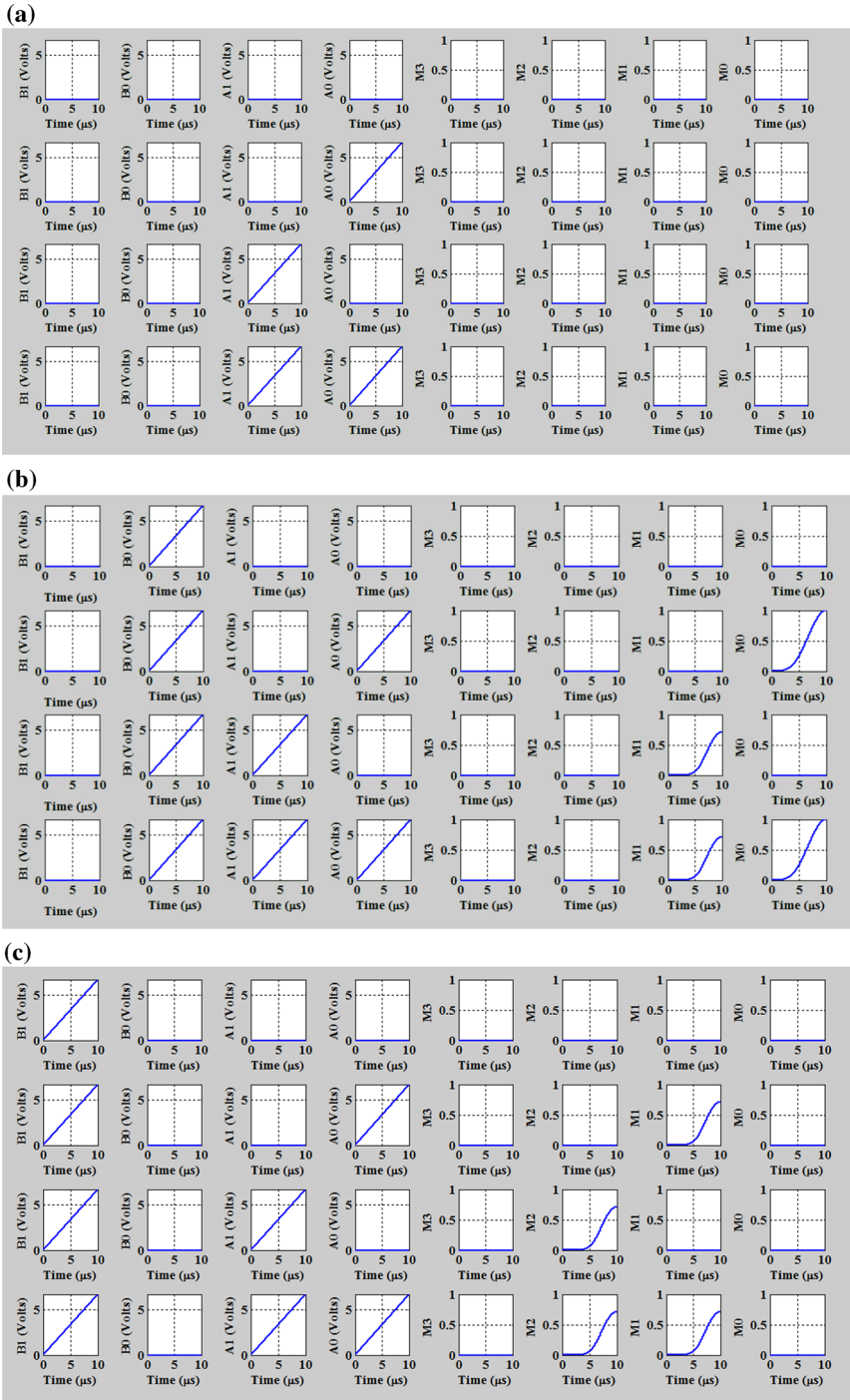
Fig. 2 MATLAB simulation results of 2-bit multiplier, when the magnitude of B is 0 (**a**), 1 (**b**), 2 (**c**), 3 (**d**) and magnitude of A changes from 0 to 3
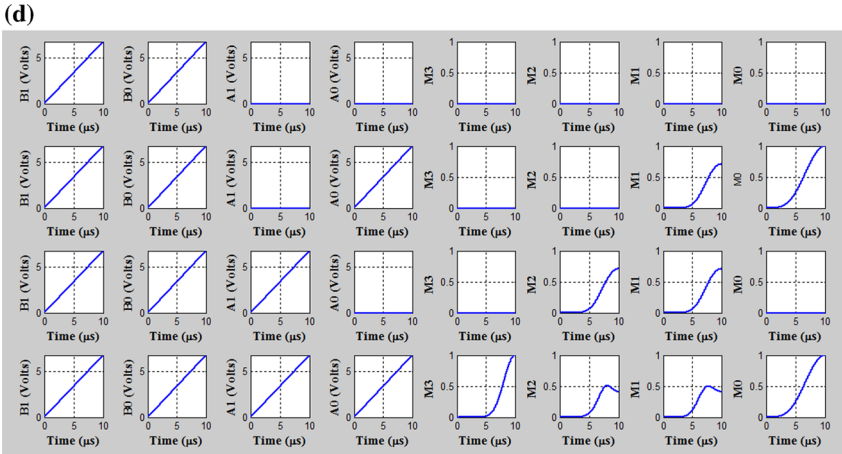
(d)

Fig. 2 continued

3.1.2 Case 2: $B_1 = 0$, $B_0 = 0$, $A_1 = 0$, $A_0 = 1$

Incoming light to MZI1 and MZI2 is reaching to first input port of MZI3 and MZI5 respectively and then terminated at their second output port because the control signal is OFF. As shown in Fig. 3a there is no light at any output port. Hence the product of 2-bit numbers for this case is being getting verified.

### 3.1.3 Case 3: $B_1 = 0$, $B_0 = 0$, $A_1 = 1$, $A_0 = 0$

Optical signals feeding to MZI1, MZI2, MZI4, and MZI6 are terminated at their second output ports because the control signals to these MZIs are LOW. Incoming optical signal to MZI9 and MZI12 are terminated at first output port of MZI11and MZI14 as shown in Fig. 1. Hence there is no optical signal at any output port as shown in Fig. 3a, which is verifying the product of 2-bit numbers.

3.1.4 Case 4: $B_1 = 0$, $B_0 = 0$, $A_1 = 1$, $A_0 = 1$

Incoming light to MZI1and MZI2 is reaching to first input port of MZI3 and MZI5 respectively and then terminated at their second output port because the control signal is OFF. As shown in Fig. 3a there is no light at any output port.

3.1.5 Case 5: $B_1 = 0$, $B_0 = 1$, $A_1 = 0$, $A_0 = 0$

Optical signals feeding to all six MZIs are terminated at the second port of MZI1, MZI2, MZI7, and MZI6 because the control signal to these MZIs are LOW. Incoming optical signal to MZI9 and MZI12 are terminated at the first output port of MZI11 and MZI14 as shown in Fig. 1. Hence there is no optical signal at any output port as shown in Fig. 3b, which verifies the product of 2-bit numbers.
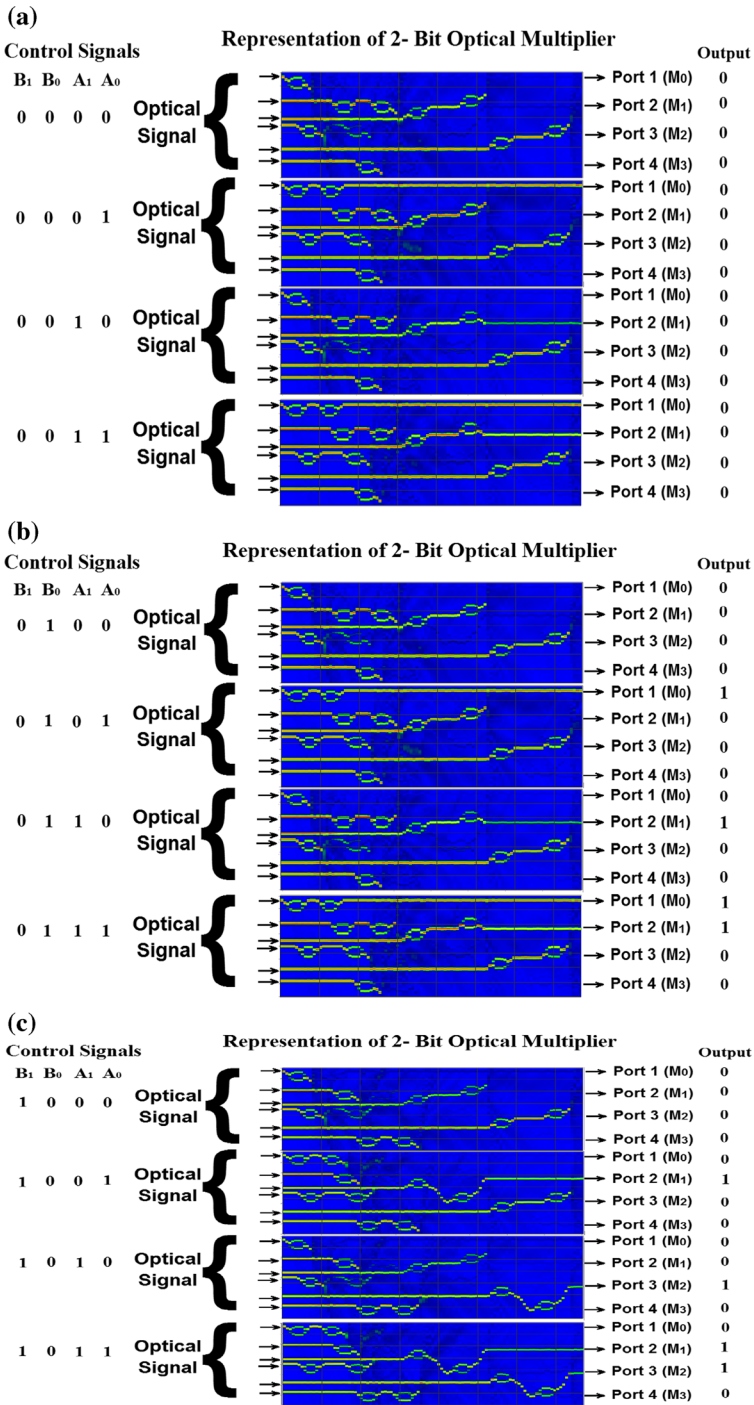
Fig. 3 The results of the 2-bit multiplier operation for different combinations of control signals obtained through the Beam propagation method, when the magnitude of B is 0 (**a**), 1 (**b**), 2 (**c**), 3 (**d**) and magnitudes A changes from 0 to 3
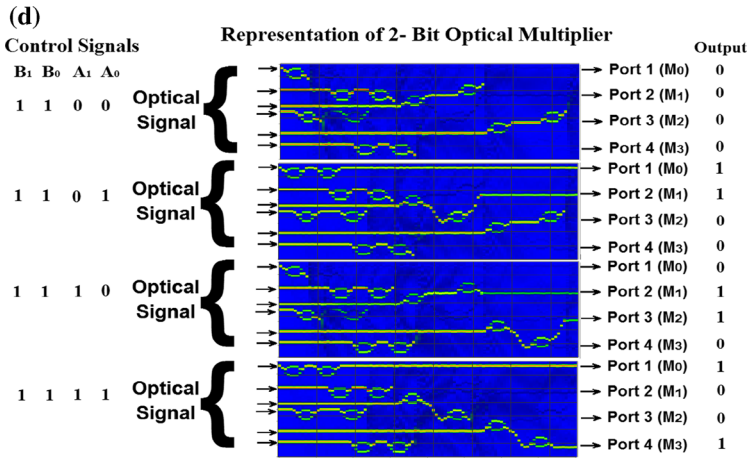
(d)

Fig. 3 continued

Table 1 Optical signal of 2-bit multiplier at the different ports due to different combination of control signals

Control signal				Optical output at different ports (B·A)			
B		A		Port 4 (M_3)	Port 3 (M_2)	Port 2 (M_1)	Port 1 (M_0)
B_1	B_0	A_1	A_0				
0	0	0	0	0	0	0	0
0	0	0	1	0	0	0	0
0	0	1	0	0	0	0	0
0	0	1	1	0	0	0	0
0	1	0	0	0	0	0	0
0	1	0	1	0	0	0	1
0	1	1	0	0	0	1	0
0	1	1	1	0	0	1	1
1	0	0	0	0	0	0	0
1	0	0	1	0	0	1	0
1	0	1	0	0	1	0	0
1	0	1	1	0	1	1	0
1	1	0	0	0	0	0	0
1	1	0	1	0	0	1	1
1	1	1	0	0	1	1	0
1	1	1	1	1	0	0	1

3.1.6 Case 6: $B_1 = 0$, $B_0 = 1$, $A_1 = 0$, $A_0 = 1$

In the presence of the signal A_0 of MZI1 and B_0 of MZI3, the incident optical signal of first input port of MZI1 appears at its first output port and then it appears at first input port of

MZI3 as shown in Fig. 1. Finally, it appears at port 1 (M_0) while there is no light reaching to rest of the output ports, which satisfies the product of B(01) and A(01) as shown in Fig. 3b.

3.1.7 Case 7: $B_1 = 0$, $B_0 = 1$, $A_1 = 1$, $A_0 = 0$

The light from the constant optical source is incident on the first input port of the MZI4 is reaching to the first output port of MZI7 which behave as the control signal for MZI11 and MZI10. At the same time input signal through MZI9 is reaching to second input port of MZI11 and finally it appears at output port 2 (M_1), which satisfies the result as shown in Fig. 3b.

3.1.8 Case 8: $B_1 = 0$, $B_0 = 1$, $A_1 = 1$, $A_0 = 1$

In the presence of control signal A_0 of MZI1 and B_0 of MZI3, the incident optical signal of first input port of MZI1 appears at the first input port of MZI3 and then finally it appears at port 1 (M_0). Also, light from the constant optical source is incident on the first input port of the MZI4 and it is reaching to the first output port of MZI7 (as $A_1 = 6.75$ V) which behaves as the control signal for MZI11 and MZI10. At the same time input signal from the first input port of MZI2 is reaching at the second output port of MZI5 (as $B_1 = 0$ V). So, control signal for MZI9 is low, and optical signal from the second input port of MZI9 is appearing at the second output port of MZI11. So, finally we get $M_1 = 1$ at Port 2 in Fig. 3b and no light at second output port of MZI13 and MZI14 respectively.

3.1.9 Case 9: $B_1 = 1$, $B_0 = 0$, $A_1 = 0$, $A_0 = 0$

Optical signals feeding to all six MZIs are terminated at the second output port of MZI1, MZI2, MZI4, and MZI6 because the control signal to these MZIs are LOW. Incoming optical signal to MZI9 and MZI12 are terminated at the first output port of MZI11 and MZI14 as shown in Fig. 1. Hence there is no optical signal at any output port as shown in Fig. 3c which verifies the product of 2-bit numbers.

3.1.10 Case 10: $B_1 = 1$, $B_0 = 0$, $A_1 = 0$, $A_0 = 1$

The light from the constant optical source is incident on the first input port of the MZI1 and terminated at second output port of MZI3 (control signal is OFF), as a result $M_0 = 0$. The incoming light to the first input port of MZI2 (control signal is ON) is reaching to first input port of MZI5 (control signal is ON) and it is working as a control signal for MZI9. So, incoming light at the second input port of MZI9 (control signal is ON) is reaching to the second input port of MZI10. Finally it appears at first output port of MZI10 (control signal is OFF) and we get $M_1 = 1$.

3.1.11 Case 11: $B_1 = 1$, $B_0 = 0$, $A_1 = 1$, $A_0 = 0$

The light emergimg from the first input port of MZI1, MZI2 and MZI4 is terminated at the second output port of MZI1, MZI2, and MZI4 respectively. (Because control signal A_0 and B_0 are OFF). So no light appears at the first output port of MZI3 (Port M_0 in Fig. 1) and at first output port of MZI10 (Port M_1 in Fig. 1). But the incoming light to the first input port

of MZI6 (control signal B_1 is ON) is reaching to first output port of MZI8 (control signal A_1 is ON), and it is working as a high control signal for MZI12. So, the light emergimg from the second input port of MZI12 is reaching to first output port of MZI13 (control signal is OFF) and no light at second output port of MZI13. So, finally we get $M_3M_2M_1M_0 = 0100$ as shown in Fig. 3c.

3.1.12 Case 12: $B_1 = 1$, $B_0 = 0$, $A_1 = 1$, $A_0 = 1$

As the control signal of MZI1 is ON ($A_0 = 6.75$ V) and control signal to MZI3 is OFF ($B_0 = 0$ V), the light from the first input port of MZI1 is terminated at the second output port of MZI3 and we get no light at first output port of MZI3 ($M_0 = 0$). The incoming light to first input port of MZI4 (control signal $B_0 = 0$ V) is also terminating at its second output port. So control signal of MZI10 and MZI11 is OFF ($X_2 = 0$ V). Also The incoming light to first input port of MZI2 (control signal $A_0 = 6.75$ V) is reaching at the first output port of MZI5 (control signal $B_1 = 6.75$ V), and it is working as a HIGH control signal (X_1) for MZI9. So the light from the second input port of MZI9 is reaching to first output port of MZI10 (control signal X_2 is OFF) and no light ($X_4 = 0$) at second output port of MZI10 and its working as an OFF control signal for MZI13 and MZI14. Also the light to the second input port of MZI12 (control signal X_3 is ON) is reaching at the first output port of MZI13 (control signal X_4 is OFF) and no light at its second output port. Finally we have $M_3M_2M_1M_0 = 0110$ as shown in Fig. 3c.

3.1.13 Case 13: $B_1 = 1$, $B_0 = 1$, $A_1 = 0$, $A_0 = 0$

Optical signals feeding to the first input port of MZI1, MZI2, MZI4 and MZI6 are terminated at the second output port of MZI1, MZI2, MZI7 and MZI8 respectively because the control signals to these MZIs are LOW. Incoming optical signal to MZI9 (control signal X_1 is OFF) and MZI12 (control signal X_3 is OFF) are terminated at first output port of MZI11 (control signal X_2 is OFF) and MZI14 (control signal X_4 is OFF) respectively. Hence there is no optical signal at any output port as shown in Fig. 1 and finally we get $M_3M_2M_1M_0 = 0000$ as shown in Fig. 3d.

3.1.14 Case 14: $B_1 = 1$, $B_0 = 1$, $A_1 = 0$, $A_0 = 1$

The light from the constant optical source is incident on the first input port of the MZI1(control signal A_0 is ON) and appears at first output port (Port M_0 in Fig. 1) of MZI3 (control signal B_0 is ON) while the incoming light to the first input port of MZI4 (control signal B_0 is ON) is terminated to the second output port of MZI7 (control signal A_1 is OFF), which makes the control signal (X_2) of MZI10 and MZI11 OFF. Light emerging from the first input port of the MZI2 (control signal A_0 is ON) appears at first output port of MZI5 (control signal B_1 is ON) and enables the control signal (X_1) of MZI9. Then the light to the second input port of MZI9 (control signal X_1 is ON) appears on the first output port of MZI10 (control signal X_2 is OFF) and no light at the second output port of MZI10 which disables the control signal (X_4) of MZI13 and MZI14. Incoming optical signal to the first input port of MZI6 (control signal B_1 is ON) is terminated at the second output port of MZI8 (control signal A_1 is OFF) and disables the control signal (X_3) of MZI12. Finally the light from the second input port of MZI12 is terminated at the first output port of MZI14

(control signal X_4 is OFF) and no optical signal at second output port of MZI14 and at the first output port of MZI13. Hence we get $M_3M_2M_1M_0 = 0011$ as shown in Fig. 3d.

3.1.15 Case 15: $B_1 = 1$, $B_0 = 1$, $A_1 = 1$, $A_0 = 0$

The light emerging from the first input port of MZI1 and MZI2 is terminated at their respective second output ports. (Because the control signal A_0 is OFF). So no light appears on the first output port of MZI3 (Port M_0 in Fig. 1) and at the first output port of MZI5, which disables the control signal (X_1) of MZI9. The light from the first input port of MZI4 and MZI6 is appeared at the first output port of MZI7 and MZI8 respectively (Because control signal A_1 and B_1 are ON). Which enables the control signal X_1 and X_3 of MZI9 and MZI12 respectively. So the light from the second input port of MZI9 (control signal X_1 is ON) is appeared at the first output port of MZI10(control signal X_2 is OFF) and the light from the second input port of MZI12 (control signal X_3 is ON) is appeared at the first output port of MZI13 (control signal X_4 is OFF) and no light at the second output port of MZI13. Hence finally we get $M_3M_2M_1M_0 = 0110$ as shown in Fig. 3d.

3.1.16 Case 16: $B_1 = 1$, $B_0 = 1$, $A_1 = 1$, $A_0 = 1$

Incoming optical signal to the first input port of MZI1 is appearing at the first output port of MZI3 (as the control signals A_0 and B_0 are ON) which results in $M_0 = 1$. The light from the first input port of MZI2 is appeared at the the first output port of MZI5 (Because control signals A_0 and B_1 are ON), which enables the control signals (X_1) of MZI9. Also the light from the first input port of MZI4 and MZI6 is appeared at the the first output port of MZI7 and MZI8 respectively (Because control signals A_1, B_0 and B_1 are ON), which enables the control signals X_2 and X_3 of MZI10, MZI11 and MZI12 respectively. So the light from the second input port of MZI9 (control signal X_1 is ON) is appearing at the second output port of MZI10 (control signal X_2 is ON) which enables the control signal (X_4) of MZI13 and MZI14, and the light from the second input port of MZI12 (control signal X_3 is ON) is appearing at the second output port of MZI13 (control signal X_4 is ON) and no light at the first output port of MZI13. So, finally we have $M_3M_2M_1M_0 = 1001$ as shown in Fig. 3d.

3.2 Scheme to generate return-to-zero (RZ) pulse format

The return-to-zero (RZ) pulse can be generated by using a continuous-wave optical source (such as DFB laser) followed by a two stage external modulator. The first stage creates a periodic train of short (RZ) pulses, and the second stage forces the modulation by blocking out the '0' bit and passing the '1' bit. This modulation is performed by using the electro-optic effect of lithium niobate (LiNbO$_3$), where an applied voltage induces a change in refractive index of the material.

In Fig. 4, two MZIs are being used to construct a two-stage modulator to produce optical RZ pulses. The continuous-wave optical source is being fed to the first input port of the MZI1. The electrical voltage pulses are applied at the second electrode of the MZI1. According to the variation of the electric clock input (voltage pulses applied at the second electrode of the MZI1), the periodic optical pulses are obtained at the first output port of the MZI1. The first and second output ports of the MZI1 are connected to the first and second input ports of the MZI2 respectively. The electrical non-return-to-zero (NRZ) data is applied to the second electrode of MZI2. The data bit '1' forces the optical pulse to
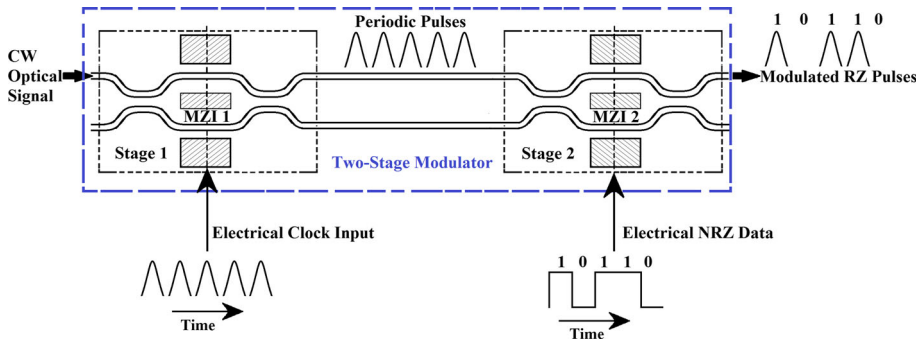
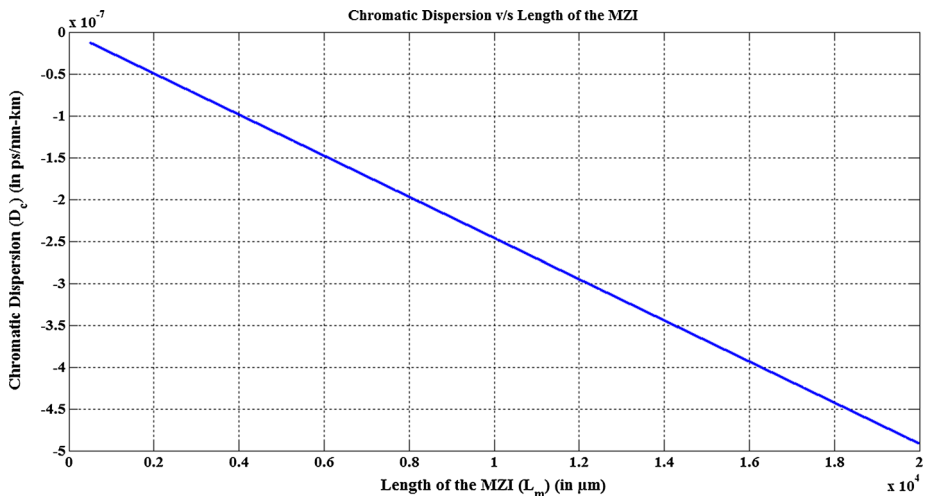**Fig. 4** Scheme to generate return to zero (RZ) pulse

Fig. 5 Variation of chromatic dispersion with respect to length of MZI

appear at the first output port of MZI2 from its first input port. Whereas the data bit '0' forces the optical pulse to appear at the second output port of MZI2 from its first input port. As a result the RZ optical pulses at the first output port of MZI2 are obtained (as shown in Fig. 4). Hence, The RZ operation of 2-bit multiplier can be accomplished by replacing each MZI of Fig. 1 (whose input port is coupled to light source) with the above system (Fig. 4). The RZ pulse format can also be generated by directly applying the mode-locked ring laser source at the input of the MZI (Zoiros et al. 2000), but it results in considerably chirped pulses.

4 Study and analysis of some factors influencing the performances of proposed device

The performance of a single MZI used in the construction of proposed device is examined by performing the 2D isotropic simulation using the paraxial BPM with finite difference engine scheme parameter of 0.5, propagation step of 1.3 μm and transparent boundary
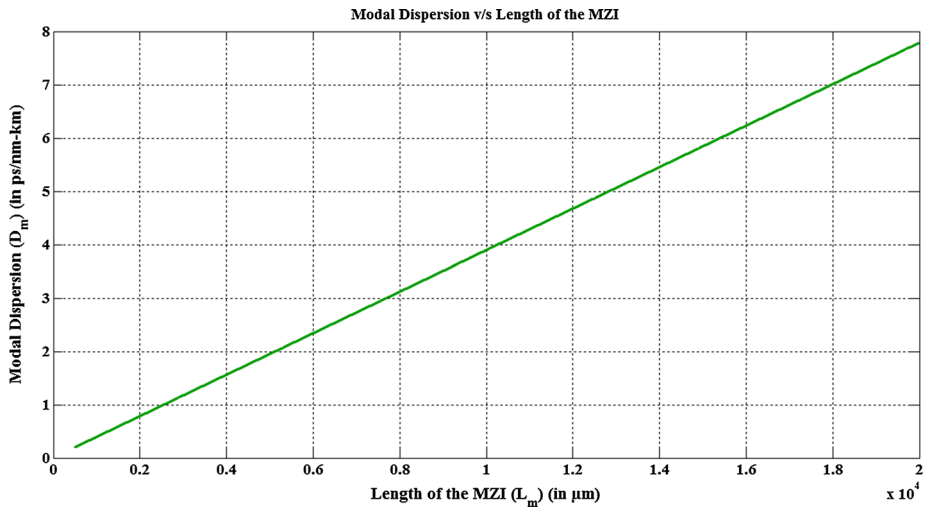
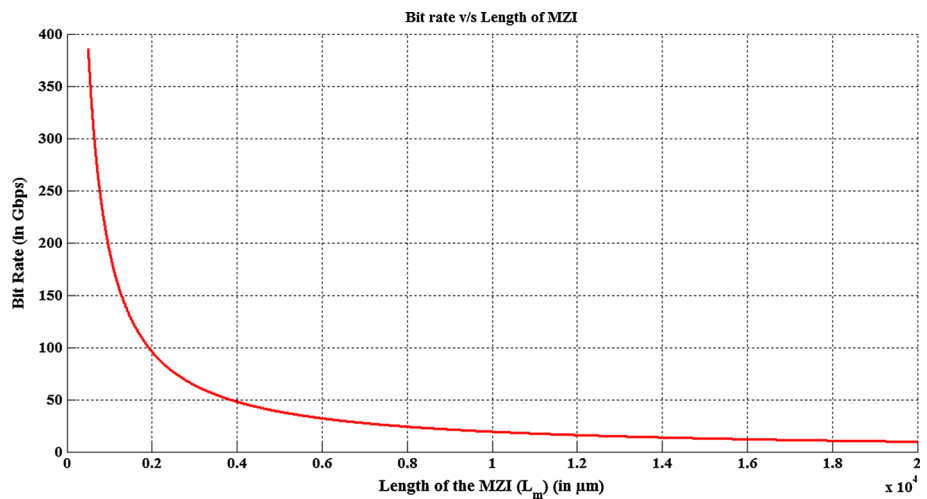**Fig. 6** Variation of modal dispersion with increase in length of MZI

Fig. 7 Variation of bit rate with respect to length of MZI

condition. The global data has been taken as refractive index MODAL and TM polarized test signals with wavelength 1.3 μm is considered. The chromatic dispersion of a single LiNbO$_3$ based MZI is given by (Kumar et al. 2015b);

$$D_c = -\left(\frac{L_m \cdot \Delta\lambda.\lambda}{c}\right) \cdot \left(\frac{d^2 n_e}{d\lambda^2}\right) \tag{5}$$

where L_m is the length of a single MZI. λ is the operating wavelength and $\Delta\lambda$ is the spectral line width of optical source. n_e is the effective refractive index of the material (LiNbO$_3$)
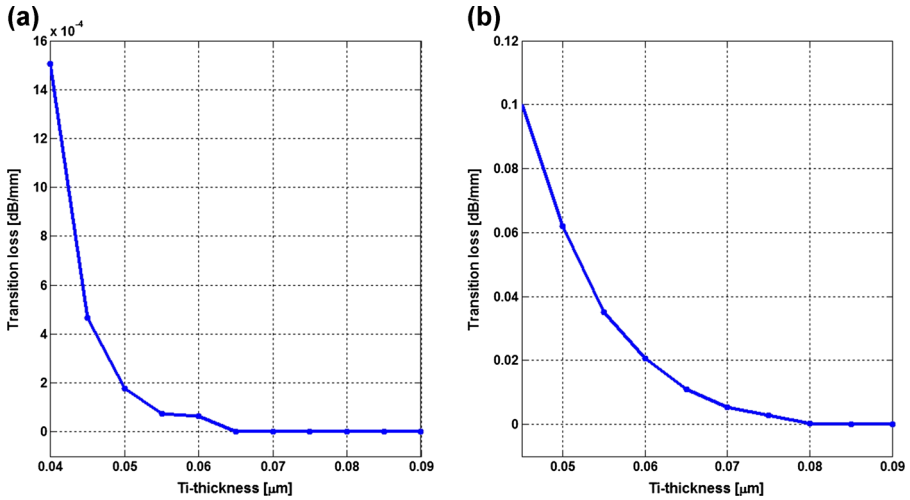
Fig. 8 Variation of loss with respect to Ti-thickness (t_s) for **a** straight waveguide and **b** curved (S-bend) waveguide for operating wavelength 1.3 μm
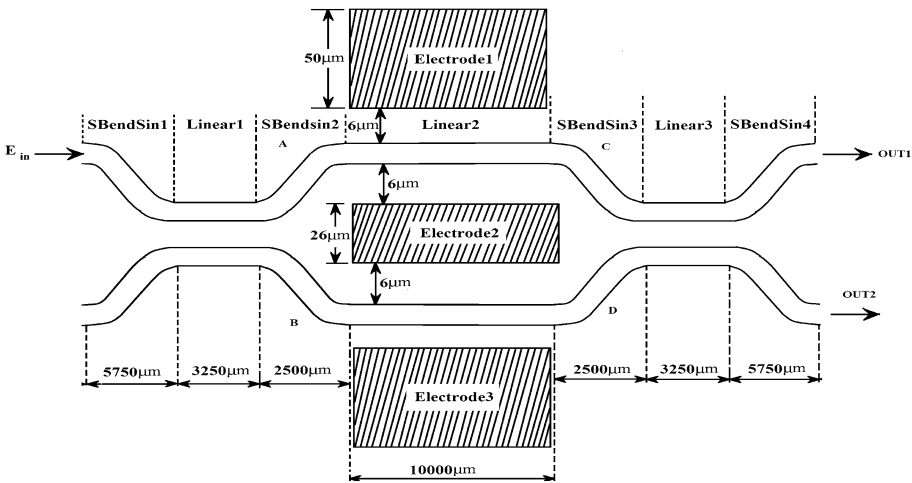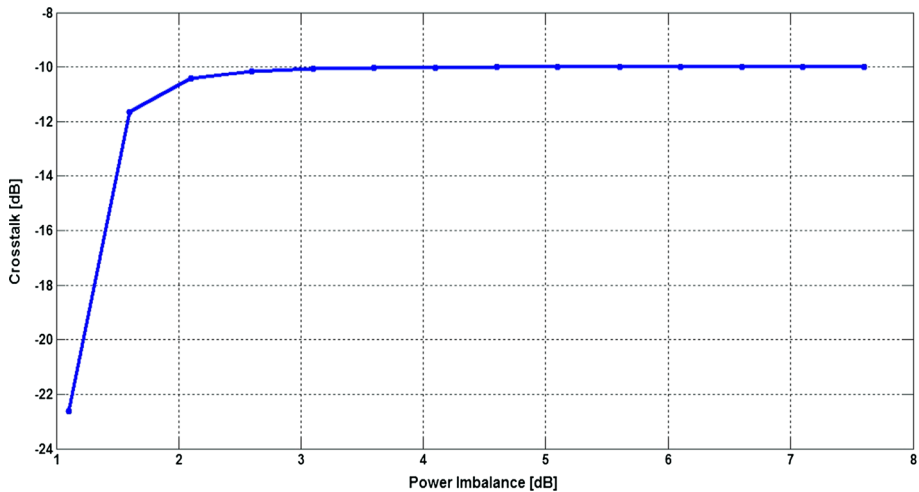

Fig. 9 Schematic view of Mach–Zehnder interferometer

MZI. The modal dispersion, D_{modal} for a multimode step-index electro-optic device with length L_m is given by

$$D_m = \frac{L_m n_e \Delta n_e}{c} \quad (6)$$

Δn_e is the relative refractive index difference. The total dispersion coefficient D_{total} is given by

$$D_{total} = D_m + D_c \quad (7)$$

Fig. 10 Representation of the cross talk level with the variation of power imbalance (switch state: cross) for operating wavelength 1.3 μm

The rise time of system in terms of bit rate (BR) for NRZ pulse is given by

$$BR = \frac{0.7}{D_{total}} \qquad (8)$$

Figure 5 shows the variation of chromatic dispersion in a single MZI at an operating wavelength of 1.3 μm, as the length of MZI is varied from 500 to 20,000 μm. It is apparent from the plot that with the increase in length of MZI, chromatic dispersion goes on increasing in negative direction. Similarly, Fig. 6 shows the variation of modal dispersion with the length of MZI.

Modal dispersion also increases with the length of MZI. Although, at smaller length, dispersion is less and pulse broadening is less. But, there is a check in reducing the length of MZI to very small values for a specified wavelength, because as the length of MZI reduces, switching voltage required for the operation of MZI increases as given by (Raghuwanshi et al. 2013)

$$V = \frac{\lambda}{n^3} \frac{\Delta\varphi}{\pi} \frac{1}{r} \frac{d}{L} \qquad (9)$$

where λ is the wavelength of light used. $\Delta\varphi$ is the phase change due to applied electric field. r is electro-optic coefficient ($\cong 36.6 \times 10^{-12}$ m/V for $LiNbO_3$). d is the separation between electrodes and L is the substantial length. Also, the available length is not sufficient to couple energy from one waveguide to other. But still, by optimizing various parameters like length of MZI, switching voltage and wavelength of operation, BR of the order of 20-200 Gbps can be obtained as shown in Fig. 7. So, by selecting appropriate length of MZI, low power consumption structure with low latency and high speed can be obtained.

The transition losses for straight and curved waveguides with the variation of Ti-diffusion thickness in the range of 0.04–0.09 μm can also be observed (Kumar et al. 2014b).
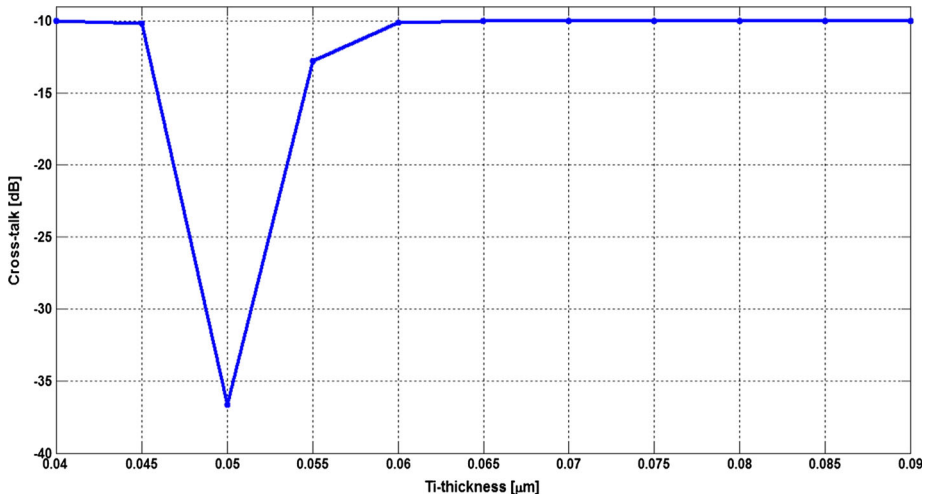
Fig. 11 Calculated cross-talk levels due to variation in Ti-thickness for operating wavelength 1.3 µm; (switch state: cross)

Figure 8 shows that these losses can be kept at low value by taking the value of $t_s \geq 0.05$ µm for the test wavelength 1.3 µm. Now, the effect of power imbalance and their impact on the crosstalk levels introduced at the end of interferometers due to the variation of the Ti thickness (t_s) has been analyzed. The power level coming out from the end of the first coupler (as shown in Fig. 9) has been monitored. The power imbalance at the output splitter can be obtained using following definitions (Singh et al. 2012).

$$PI = 10 \log\left(\frac{A}{B}\right) \tag{10}$$

where A and B are the optical signal strength at the end of the first coupler (as shown in Fig. 9). Hence, cross talk at the end of the interferometer arms is,

$$CT = 10 \log \frac{\left[\left(\frac{C}{2}\right)^{1/2} - \left(\frac{D}{2}\right)^{1/2}\right]^2}{\left[\left(\frac{C}{2}\right)^{1/2} + \left(\frac{D}{2}\right)^{1/2}\right]^2} \tag{11}$$

Since, C and D are power levels at the end of the interferometer arms and it can be expressed as follows

$$C = \frac{1}{10^{PI/10} + 1} \quad \text{and} \quad D = 1 - C \tag{12}$$

On the basis of the Eqs. (6)–(8) the analysis has been obtained for the basic MZI used for the proposed device. Figure 10 projects that crosstalk levels at the end of the interferometer arms becomes worst as the power imbalance increases.

Figure 11 shows the variation in crosstalk generated at the interferometers of the two arms due to the variation of the Ti-thickness in the range of 0.04–0.09 µm. On the basis of the Fig. 11, the low crosstalk can be obtained as -36.67 dB at the Ti-thickness of 0.05 µm for the operating wavelength of 1.3 µm. It is examined that switch operation is more stable
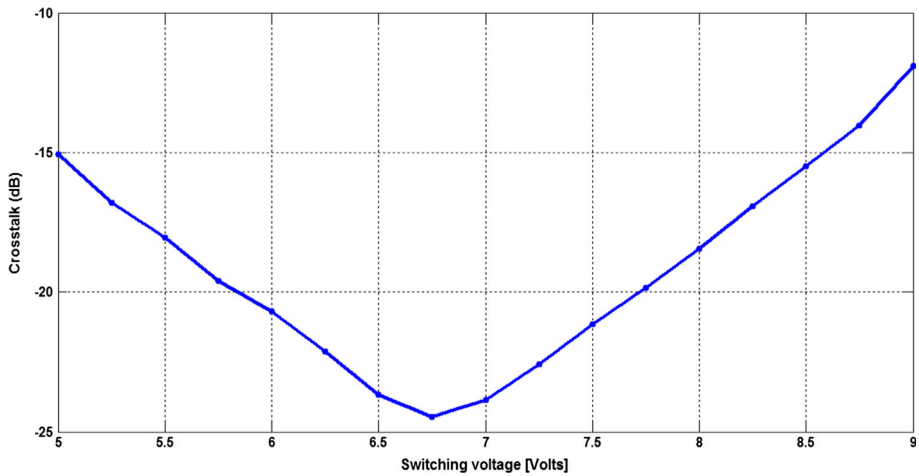
Fig. 12 Calculated cross-talk levels of the switch (in bar state) as a variation of switching voltage for $\lambda = 1.3$ μm (with $t_s = 0.05$ μm)

for lateral diffusion length $D_H = 3.5$ μm and diffusion length in depth $D_V = 4.2$ μm. However, the switch is forced to obtain its bar state due to EO effect, by applying the voltage across the electrode in the range of 5–9 V.

Figure 12 shows the variation in the cross-talk generated at the interferometer arms due to the variation in the switching voltage in its bar state. According to the Fig. 12, it is cleared that switching performance gives the best result for 6.75 V for the test wavelength of 1.3 μm. It can be observed that, for the switching voltage 6.75 V the crosstalk is −24.47 dB. Basically, the ON/OFF extinction ratio (ER) should be large for optical modulator used in the digital communication system. The ER between the optical intensity at the ON-state and at the OFF-state is determined by the optical balance between the two arms. It can be calculated as follow (Li and Yu 2003):

$$ER = \frac{(OUT_1 + OUT_2)^2}{(OUT_1 - OUT_2)^2} \tag{13}$$

The ratio of $(OUT_1/OUT_2)^2$ represents the optical power difference between the two arms, which can be caused by different optical loss in the two arms, as well as the imbalance in the optical splitter and combiner and the Ti-diffusion thickness and switching voltage.

Figure 13 represents the plot of the ER versus the power difference. From the Fig. 13, it is seen that in order to achieve more than 20 dB ER, the power difference has to be <0.8 dB. The analysis is carried out to examine the behavior of ER with respect to switching voltage and Ti-thickness. Figure 14a represents the variation of ER with the variation of Ti-thickness and Fig. 14b shows the variation of ER with switching voltage. The analysis is carried out for checking the suitability of Ti-thickness and switching voltage in order to achieve the satisfactory ER. The high value of ER can be obtained at specified Ti-thickness and switching voltage. The single MZI of proposed device shows the ER of 39.27 dB at Ti-thickness of 0.05 μm and switching voltage of 6.75 V.
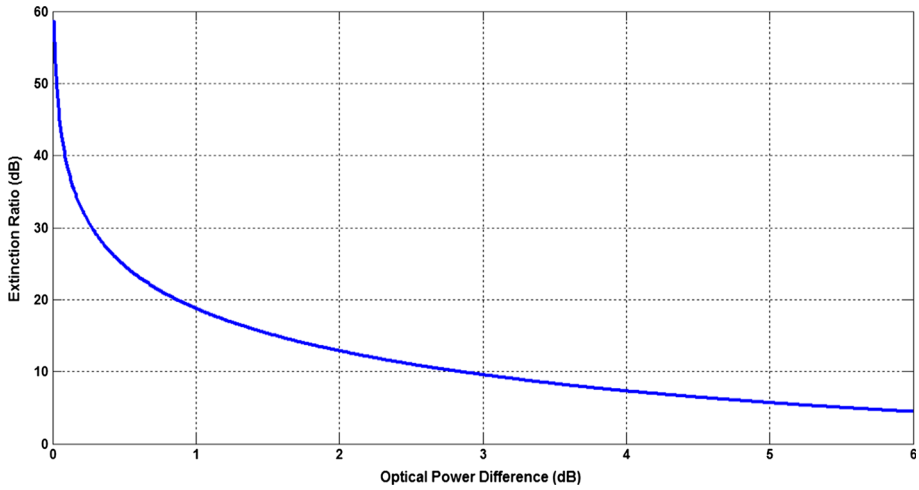
Fig. 13 Extinction ratio for an modulator versus the optical power difference between its two arms
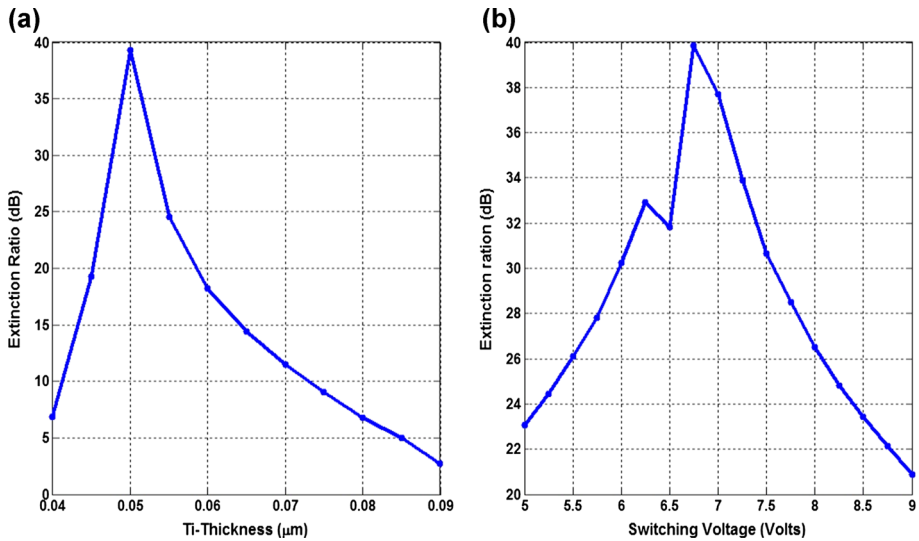
Fig. 14 Variation of extinction ratio with the variation of **a** Ti-thickness **b** switching voltage, for $\lambda = 1.3\ \mu m$

5 Conclusion

The important aspects of electro-optic effect based Mach–Zehnder interferometer as an optical switch is presented. The layout diagram of the proposed devices is discussed with the appropriate mathematical analysis and the results are obtained using the MATLAB simulation. The discussed method to implement the proposed device is verified using the BPM. The paper includes detailed discussion of the multiplier. It presents the guideline to realize 2-bit multiplier by using MZIs. The analysis of various factors such as BR,

crosstalk, ER, power imbalance and transition loss has been presented. The results furnished in this paper will be a stepping stone in the area of designing optical computing devices for optical network systems.

Appendix

For all possible minterms at first output port of MZI3 (Port M_0 in Fig. 1), the normalized power (for M_0) is calculated as follows;

Using the relation for single stage MZI structure in (Kumar et al. 2014b) we can write,

$$\text{OUT1}_{\text{MZI3}} = \left[\left\{ -j e^{-j(\varphi_{0\text{MZI1}})} \sin\left(\frac{\Delta\varphi_{\text{MZI1}}}{2}\right) \right\} \left\{ -j e^{-j(\varphi_{0\text{MZI3}})} \sin\left(\frac{\Delta\varphi_{\text{MZI3}}}{2}\right) \right\} \right] E_{in} \quad (14)$$

$$\frac{\text{OUT1}_{\text{MZI3}}}{E_{in}} = \left[\left\{ -j e^{-j(\varphi_{0\text{MZI1}})} \sin\left(\frac{\Delta\varphi_{\text{MZI1}}}{2}\right) \right\} \left\{ -j e^{-j(\varphi_{0\text{MZI3}})} \sin\left(\frac{\Delta\varphi_{\text{MZI3}}}{2}\right) \right\} \right] \quad (15)$$

$$M_0 = \left| \frac{\text{OUT1}_{\text{MZI3}}}{E_{in}} \right|^2 = \left\{ \sin^2\left(\frac{\Delta\varphi_{\text{MZI1}}}{2}\right) \sin^2\left(\frac{\Delta\varphi_{\text{MZI3}}}{2}\right) \right\} \quad (16)$$

In the same manner, for M_1, the normalized power at first output port of MZI10 (Port M_1 in Fig. 1) is calculated as follows;

$$\text{OUT1}_{\text{MZI10}} = \left[\left\{ -j e^{-j(\varphi_{0\text{MZI9}})} \sin\left(\frac{\Delta\varphi_{\text{MZI9}}}{2}\right) \right\} \left\{ j e^{-j(\varphi_{0\text{MZI10}})} \cos\left(\frac{\Delta\varphi_{\text{MZI10}}}{2}\right) \right\} \right] E_{in} \quad (17)$$

$$\frac{\text{OUT1}_{\text{MZI10}}}{E_{in}} = \left[\left\{ -j e^{-j(\varphi_{0\text{MZI9}})} \sin\left(\frac{\Delta\varphi_{\text{MZI9}}}{2}\right) \right\} \left\{ j e^{-j(\varphi_{0\text{MZI10}})} \cos\left(\frac{\Delta\varphi_{\text{MZI10}}}{2}\right) \right\} \right] \quad (18)$$

$$\left| \frac{\text{OUT1}_{\text{MZI10}}}{E_{in}} \right|^2 = \left\{ \sin^2\left(\frac{\Delta\varphi_{\text{MZI9}}}{2}\right) \cos^2\left(\frac{\Delta\varphi_{\text{MZI10}}}{2}\right) \right\} \quad (19)$$

and the normalized power at the second output port of MZI11 is calculated as follows;

$$\text{OUT2}_{\text{MZI11}} = \left[\left\{ j e^{-j(\varphi_{0\text{MZI9}})} \cos\left(\frac{\Delta\varphi_{\text{MZI9}}}{2}\right) \right\} \left\{ -j e^{-j(\varphi_{0\text{MZI11}})} \sin\left(\frac{\Delta\varphi_{\text{MZI11}}}{2}\right) \right\} \right] E_{in} \quad (20)$$

$$\frac{\text{OUT2}_{\text{MZI11}}}{E_{in}} = \left[\left\{ j e^{-j(\varphi_{0\text{MZI9}})} \cos\left(\frac{\Delta\varphi_{\text{MZI9}}}{2}\right) \right\} \left\{ -j e^{-j(\varphi_{0\text{MZI11}})} \sin\left(\frac{\Delta\varphi_{\text{MZI11}}}{2}\right) \right\} \right] \quad (21)$$

$$\left| \frac{\text{OUT1}_{\text{MZI11}}}{E_{in}} \right|^2 = \left\{ \cos^2\left(\frac{\Delta\varphi_{\text{MZI9}}}{2}\right) \sin^2\left(\frac{\Delta\varphi_{\text{MZI11}}}{2}\right) \right\} \quad (22)$$

Hence for M_1, the normalized power at Port M_1 (in Fig. 1) is calculated as follows;

$$M_1 = \left\{ \sin^2\left(\frac{\Delta\varphi_{MZI9}}{2}\right) \cos^2\left(\frac{\Delta\varphi_{MZI10}}{2}\right) \right\} + \left\{ \cos^2\left(\frac{\Delta\varphi_{MZI9}}{2}\right) \sin^2\left(\frac{\Delta\varphi_{MZI11}}{2}\right) \right\} \quad (23)$$

Similarly for M_2, the normalized power at first output port of MZI13 (Port M_2 in Fig. 1) is calculated as follows;

$$OUT1_{MZI13} = \left[\left\{ -je^{-j(\varphi_{0MZI12})} \sin\left(\frac{\Delta\varphi_{MZI12}}{2}\right) \right\} \left\{ je^{-j(\varphi_{0MZI13})} \cos\left(\frac{\Delta\varphi_{MZI13}}{2}\right) \right\} \right] E_{in} \quad (24)$$

$$\frac{OUT1_{MZI13}}{E_{in}} = \left[\left\{ -je^{-j(\varphi_{0MZI12})} \sin\left(\frac{\Delta\varphi_{MZI12}}{2}\right) \right\} \left\{ je^{-j(\varphi_{0MZI13})} \cos\left(\frac{\Delta\varphi_{MZI13}}{2}\right) \right\} \right] \quad (25)$$

$$\left| \frac{OUT1_{MZI13}}{E_{in}} \right|^2 = \left\{ \sin^2\left(\frac{\Delta\varphi_{MZI12}}{2}\right) \cos^2\left(\frac{\Delta\varphi_{MZI13}}{2}\right) \right\} \quad (26)$$

and the normalized power at the second output port of MZI14 is calculated as follows;

$$OUT2_{MZI14} = \left[\left\{ je^{-j(\varphi_{0MZI12})} \cos\left(\frac{\Delta\varphi_{MZI12}}{2}\right) \right\} \left\{ -je^{-j(\varphi_{0MZI14})} \sin\left(\frac{\Delta\varphi_{MZI14}}{2}\right) \right\} \right] E_{in} \quad (27)$$

$$\frac{OUT2_{MZI14}}{E_{in}} = \left[\left\{ je^{-j(\varphi_{0MZI12})} \cos\left(\frac{\Delta\varphi_{MZI12}}{2}\right) \right\} \left\{ -je^{-j(\varphi_{0MZI14})} \sin\left(\frac{\Delta\varphi_{MZI14}}{2}\right) \right\} \right] \quad (28)$$

$$\left| \frac{OUT2_{MZI14}}{E_{in}} \right|^2 = \left\{ \cos^2\left(\frac{\Delta\varphi_{MZI12}}{2}\right) \sin^2\left(\frac{\Delta\varphi_{MZI14}}{2}\right) \right\} \quad (29)$$

Hence for M_2, the normalized power at Port M_2 (in Fig. 1) is calculated as follows;

$$M_2 = \left\{ \sin^2\left(\frac{\Delta\varphi_{MZI12}}{2}\right) \cos^2\left(\frac{\Delta\varphi_{MZI13}}{2}\right) \right\} + \left\{ \cos^2\left(\frac{\Delta\varphi_{MZI12}}{2}\right) \sin^2\left(\frac{\Delta\varphi_{MZI14}}{2}\right) \right\} \quad (30)$$

For all possible minterms at second output port of MZI13 (Port M_3 in Fig. 1), the normalized power (for M_3) is calculated as follows;

$$OUT2_{MZI13} = \left[\left\{ -je^{-j(\varphi_{0MZI12})} \sin\left(\frac{\Delta\varphi_{MZI12}}{2}\right) \right\} \left\{ -je^{-j(\varphi_{0MZI13})} \sin\left(\frac{\Delta\varphi_{MZI13}}{2}\right) \right\} \right] E_{in} \quad (31)$$

$$\frac{OUT2_{MZI13}}{E_{in}} = \left[\left\{ -je^{-j(\varphi_{0MZI12})} \sin\left(\frac{\Delta\varphi_{MZI12}}{2}\right) \right\} \left\{ -je^{-j(\varphi_{0MZI13})} \sin\left(\frac{\Delta\varphi_{MZI13}}{2}\right) \right\} \right] \quad (32)$$

$$M_3 = \left| \frac{OUT2_{MZI13}}{E_{in}} \right|^2 = \left\{ \cos^2\left(\frac{\Delta\varphi_{MZI12}}{2}\right) \sin^2\left(\frac{\Delta\varphi_{MZI13}}{2}\right) \right\} \quad (33)$$

For calculation of Eqs. (14)–(33), we have assumed,

$$
\left.
\begin{array}{ll}
\varphi_{0MZI1} = \dfrac{\varphi_{1MZI1} + \varphi_{2MZI1}}{2} & \Delta\varphi_{MZI1} = \varphi_{1MZI1} - \varphi_{2MZI1} = \dfrac{\pi}{V_\pi}A_0 \\[8pt]
\varphi_{0MZI2} = \dfrac{\varphi_{1MZI2} + \varphi_{2MZI2}}{2} & \Delta\varphi_{MZI2} = \varphi_{1MZI2} - \varphi_{2MZI2} = \dfrac{\pi}{V_\pi}A_0 \\[8pt]
\varphi_{0MZI3} = \dfrac{\varphi_{1MZI3} + \varphi_{2MZI3}}{2} & \Delta\varphi_{MZI3} = \varphi_{1MZI3} - \varphi_{2MZI3} = \dfrac{\pi}{V_\pi}B_0 \\[8pt]
\varphi_{0MZI4} = \dfrac{\varphi_{1MZI4} + \varphi_{2MZI4}}{2} & \Delta\varphi_{MZI4} = \varphi_{1MZI4} - \varphi_{2MZI4} = \dfrac{\pi}{V_\pi}B_0 \\[8pt]
\varphi_{0MZI5} = \dfrac{\varphi_{1MZI5} + \varphi_{2MZI5}}{2} & \Delta\varphi_{MZI5} = \varphi_{1MZI5} - \varphi_{2MZI5} = \dfrac{\pi}{V_\pi}B_1 \\[8pt]
\varphi_{0MZI6} = \dfrac{\varphi_{1MZI6} + \varphi_{2MZI6}}{2} & \Delta\varphi_{MZI6} = \varphi_{1MZI6} - \varphi_{2MZI6} = \dfrac{\pi}{V_\pi}B_1 \\[8pt]
\varphi_{0MZI7} = \dfrac{\varphi_{1MZI7} + \varphi_{2MZI7}}{2} & \Delta\varphi_{MZI7} = \varphi_{1MZI7} - \varphi_{2MZI7} = \dfrac{\pi}{V_\pi}A_1 \\[8pt]
\varphi_{0MZI8} = \dfrac{\varphi_{1MZI8} + \varphi_{2MZI8}}{2} & \Delta\varphi_{MZI8} = \varphi_{1MZI8} - \varphi_{2MZI8} = \dfrac{\pi}{V_\pi}A_1 \\[8pt]
\varphi_{0MZI9} = \dfrac{\varphi_{1MZI9} + \varphi_{2MZI9}}{2} & \Delta\varphi_{MZI9} = \varphi_{1MZI9} - \varphi_{2MZI9} = \dfrac{\pi}{V_\pi}X_1 \\[8pt]
\varphi_{0MZI10} = \dfrac{\varphi_{1MZI10} + \varphi_{2MZI10}}{2} & \Delta\varphi_{MZI10} = \varphi_{1MZI10} - \varphi_{2MZI10} = \dfrac{\pi}{V_\pi}X_2 \\[8pt]
\varphi_{0MZI11} = \dfrac{\varphi_{1MZI11} + \varphi_{2MZI11}}{2} & \Delta\varphi_{MZI11} = \varphi_{1MZI11} - \varphi_{2MZI11} = \dfrac{\pi}{V_\pi}X_2 \\[8pt]
\varphi_{0MZI12} = \dfrac{\varphi_{1MZI12} + \varphi_{2MZI12}}{2} & \Delta\varphi_{MZI12} = \varphi_{1MZI12} - \varphi_{2MZI12} = \dfrac{\pi}{V_\pi}X_3 \\[8pt]
\varphi_{0MZI3} = \dfrac{\varphi_{1MZI13} + \varphi_{2MZI13}}{2} & \Delta\varphi_{MZI13} = \varphi_{1MZI13} - \varphi_{2MZI13} = \dfrac{\pi}{V_\pi}X_4 \\[8pt]
\varphi_{0MZI14} = \dfrac{\varphi_{1MZI14} + \varphi_{2MZI14}}{2} & \Delta\varphi_{MZI14} = \varphi_{1MZI9} - \varphi_{2MZI14} = \dfrac{\pi}{V_\pi}X_4
\end{array}
\right\} \quad (34)
$$

φ_{1MZI1}, φ_{1MZI2}, φ_{1MZI3}, φ_{1MZI4}, φ_{1MZI5}, φ_{1MZI6}, φ_{1MZI7}, φ_{1MZI8}, φ_{1MZI9}, φ_{1MZI10}, φ_{1MZI11}, φ_{1MZI12}, φ_{1MZI13}, φ_{1MZI14} are the phase angle generated at the arm of MZI4, MZI5, MZI6, MZI7, MZI8, MZI9, MZI10, MZI11, MZI12, MZI13 and MZI14 respectively.

φ_{2MZI1}, φ_{2MZI2}, φ_{2MZI3}, φ_{2MZI4}, φ_{2MZI5}, φ_{2MZI6}, φ_{2MZI7}, φ_{2MZI8}, φ_{2MZI9}, φ_{2MZI10}, φ_{2MZI11}, φ_{2MZI12}, φ_{2MZI13}, φ_{2MZI14} are the phase angle generated at the lower arm of MZI1, MZI2, MZI3, MZI4, MZI5, MZI6, MZI7, MZI8, MZI9, MZI10, MZI11, MZI12, MZI13 and MZI14 respectively.

Also $X_1 = (B_1 \cdot A_0)$, $X_2 = (B_0 \cdot A_1)$, $X_3 = (B_1 \cdot A_1)$ and $X_4 = (X_1 \cdot X_2)$.

The MZI1 and MZI2 are controlled by signal A0 (the voltage applied at the second electrode, keeping other two electrodes at the ground potential). Similarly, MZI3 and MZI4 are controlled by control signal B_0.

MZI5 and MZI6 are controlled by control signal B_1.
MZI7 and MZI8 are controlled by control signal A_1.
MZI9 is controlled by control signal X_1.
MZI10 and MZI11 are controlled by control signal X_2.
MZI12 is controlled by the control signal X_3.
MZI13 and MZI14 are controlled by control signal X_4.

Basically, the control signals are 0 (0.00 V) and 1 (6.75 V) at the second electrodes of each MZI.

References

Gayen, D.K., Chattopadhyay, T., Pal, R.K., Roy, J.N.: All-optical multiplication with the help of semi-conductor optical amplifier-assisted Sagnac switch. J. Comput. Electron. **9**(2), 57–67 (2010)

Jin, H., Liu, F.M., Xu, P., Xia, J.L., Zhong, M.L., Yuan, Y., Zhou, J.W., Gong, Y.X., Wang, W., Zhu, S.N.: On-chip generation and manipulation of entangled photons based on reconfigurable lithium-niobate waveguide circuits. Phys. Rev. Lett. **113**, 103601–103605 (2014)

Kumar, S., Raghuwanshi, S.K., Kumar, A.: Implementation of optical switches by using mach–zehnder interferometer. Opt. Eng. **52**(9), 097106 (2013)

Kumar, A., Kumar, S., Raghuwanshi, S.K.: Implementation of full-adder and full-subtractor based on electro-optic effect in mach–zehnder interferometer. Opt. Commun. **324**, 93–107 (2014a)

Kumar, A., Kumar, S., Raghuwanshi, S.K.: Implementation of XOR/XNOR and AND logic gates using mach–zehnder interferometers. Optik **125**, 5764–5767 (2014b)

Kumar, S., Bisht, A., Singh, G., Choudhary, K., Sharma, D.: Implementation of wavelength selector based on electro-optic effect in Mach–Zehnder interferometers for high speed communications. Opt. Commun. **350**, 108–118 (2015a)

Kumar, S., Singh, G., Bisht, A.: 4 × 4 signal router based on electro-optic effect of mach–zehnder interferometer for wavelength division multiplexing applications. Opt. Commun. **353**, 17–26 (2015b)

Li, G.L., Yu, P.K.L.: Optical intensity modulators for digital and analog applications. J. Lightwave Technol. **21**(9), 2010–2030 (2003)

Li, G., Qian, F., Ruan, H., Liu, L.: Compact parallel optical modified-signed-digit arithmetic-logic array processor with electron-trapping device. Appl. Opt. **38**(23), 5039–5045 (1999)

Li, Q., Zhu, M., Li, D., Zhang, Z., Wei, Y., Hu, M., Zhou, X., Tang, X.: Optical logic gates based on electro-optic modulation with Sagnac interferometer. Appl. Opt. **53**(21), 4708–4715 (2014)

Mandal, D., Mandal, S., Garai, S.K.: A new approach of developing all-optical two-bit-binary data multi-plier. Opt. Laser Technol. **64**, 292–301 (2014)

Mukhopadhyay, S., Das, D.N., Das, P.P., Ghosh, P.: Implementation of all-optical digital matrix multipli-cation scheme with nonlinear material. Opt. Eng. **40**(9), 1998–2002 (2001)

Raghuwanshi, S.K., Kumar, A., Kumar, S.: 1 × 4 signal router using 3-Mach-Zhender interferometers. Opt. Eng. **52**(03), 035002 (2013)

Raghuwanshi, S.K., Kumar, A., Chen, N.K.: Implementation of sequential logic circuits using the Mach–Zehnder interferometer structure based on electro-optic effect. Opt. Commun. **333**, 193–208 (2014)

Shen, Z.Y., Wu, L.L.: Reconfigurable optical logic unit with a terahertz optical asymmetric demultiplexer and electro-opticswitches. Appl. Opt. **47**(21), 3737–3742 (2008)

Singh, G., Janyani, V., Yadav, R.P.: Modeling of a high performance Mach–Zehnder interferometer all optical switch. Optica Applicata **42**, 613–625 (2012)

Sokoloff, J.P., Prucnal, P.R., Glesk, I., Kane, M.: A terahertz optical asymmetric demultiplexer (TOAD). IEEE Photonics Technol. Lett. **5**(7), 787–789 (1993)

Vikram, C.S., Caulfield, H.J.: Position-sensing detector for logical operations using incoherent light. Opt. Eng. **44**, 115201–115204 (2005)

Wang, B.C., Baby, V., Tong, W., Xu, L., Friedman, M., Runser, R.J., Glesk, I., Pruncnal, P.R.: A novel fast optical switch based on two cascaded terahertz asymmetric demultiplexers (TOAD). Opt. Express **10**(1), 15–23 (2002)

Wooten, E.L., Kissa, K.M., Yan, A.Y., Murphy, E.J., Lafaw, D.A., Hallemeier, P.F., Maack, D., Attanasio, D.V., Fritz, D.J., McBrien, G.J., Bossi, D.E.: A review of lithium niobate modulators for fiber-optic communications systems. IEEE J. Sel. Top. Quantum Electron. **6**(1), 69–82 (2000)

Zoiros, K.E., Stathopoulos, T., Vlachos, K., Hatziefremidis, A., Houbavlis, T., Papakyriakopoulos, T., Avramopoulos, H.: Experimental and theoretical studies of a high repetition rate fiber laser, mode-locked by external optical modulation. Opt. Commun. **180**, 301–315 (2000)